Draft version December 10, 2019
Typeset using LaTeX **preprint** style in AASTeX62

Star Formation Histories of Low-Redshift Green Valley Galaxies

Peyton Benac[1]

[1]*Harvard College, Astronomy 98, Fall 2019*

ABSTRACT

In between the conventional categories of quiescent red-sequence galaxies and star-forming blue-cloud galaxies, there is a third group of galaxies that inhabit a region on the color-magnitude diagram known as the green valley. Quantifying the star formation histories of galaxies in the green valley allows us to make inferences about their evolutionary tracks. In this paper we use spectral energy distribution fitting to measure non-parametric star formation histories and other key parameters that quantify a galaxy's current star formation. We make use of data from the GALEX-SDSS-WISE Legacy Catalog, and select galaxies that also have spatially-resolved spectroscopic data from SDSS/MaNGA to enable further analysis of where star formation is taking place within these galaxies. We compare classifications by color to classifications by the specific star formation rate to test the accuracy of color as an indicator of star formation. Among the green valley galaxies, we find that 28% are quiescent, 49% are transitional, and 23% are actively star-forming.

1. INTRODUCTION

Conventionally, galaxies have been understood to primarily fall into two categories: those which are star forming and blue, and those which are quiescent and red (Baldry et al. 2004). However, the process by which galaxies transition between these stages is not well understood. Additionally, it is possible that the observed color of a galaxy is not always indicative of its star formation. Quantifying star formation in nearby ($z \leq 0.14$) galaxies can help us understand the stages of the galactic life cycle, both for these galaxies and potentially their high-redshift progenitors.

There is a third category of galaxies called the "green valley". This refers to galaxies that are green in color, and have conventionally been assumed to represent an intermediate stage between the young, blue, star-forming galaxies and the older, red, quiescent galaxies. It seems logical to assume that these galaxies may be star-forming galaxies experiencing quenching, where they are gradually moving to be more and more red as their hot, blue stars die out over time. However, classifying galaxies as belonging to this green valley based only on color fails to take into account other important information like the dust attenuation and the metallicity of the stellar population. It is possible that star-forming galaxies with high levels of dust attenuation may appear in the green valley despite truly being in the same evolutionary stage as much bluer galaxies. Color is therefore, by itself, an insufficent measure of star formation activity. However, other methods, like the spectral energy distribution (SED) fitting procedure used in this paper, can provide more information about the star formation rates.

Studying the star formation rates over time (also known as star formation histories) of green valley galaxies can illuminate whether the green valley galaxies are increasing their star formation rates

("rejuvenating") or decreasing them ("quenching"). We would also like to know the timescales involved: how quickly are the green valley galaxies changing their star formation rates relative to their star-forming or quiescent counterparts? By fitting for non-parametric star formation histories (SFH), we aim to study the evolutionary course of these galaxies without introducing the systematic errors inherent in parametric SFH fitting. Non-parametric SFH are especially useful to study rejuvenation and quenching of star-formation, because most parametric models can't accurately capture these changes.

Additionally, using the spatially resolved spectra obtained from SDSS MaNGA (Bundy et al. 2015), we would like to understand how the change in the star-formation histories is related to the spatially resolved distribution of star formation, as determined by the H-α emission. We expect, from cosmological models, that rejuvenating galaxies have centrally-concentrated star formation, and that quenching galaxies have more extended regions of star formation (Tacchella et al. 2016).

We accomplish this by using Prospector (Johnson & Leja 2017) to fit the spectral energy distributions (SED) of galaxies from the GSWLC (GALEX-SDSS-WISE) Deep catalog (Salim et al. 2016, 2018). The multi-wavelength observations in GSWLC allow us to perform SED fits that determine stellar masses, star formation rates, star formation histories, dust attenuation, and metallicity. Additionally, the non-parametric star formation histories produced by our model allow us to draw conclusions about which galaxies are quenching or rejuvenating.

The format of this paper is as follows: Section 2 describes the observational catalogs used for this analysis. Section 3 describes the physical model of a galaxy used for our fitting. Section 4 describes the parameters and priors used for fitting. Section 5 describes the results from the fit, Section 6 discusses the implications of this work, and Section 7 summarizes.

2. OBSERVATIONAL DATA

2.1. *GALEX-SDSS-WISE Legacy Catalog*

The GALEX-SDSS-WISE Legacy Catalog contains multi-wavelength photometry and physical properties derived from SED fitting for 700,000 galaxies within a redshift of 0.3 (Salim et al. 2016, 2018). This catalog provides the necessary fluxes at a variety of wavelengths that we can then pass to the SED fitting pipeline and determine our own derived properties. The physical properties calculated by Salim et al. (2018) provide values against which we can compare our own derived values. The bands in which we have photometry from this catalog are GALEX NUV and FUV, SDSS ugriz, 2MASS HJK, and WISE 1, 2, 3, and 4, spanning a range of wavelengths from 135 nm to 22 μm. The errors on the WISE photometry seemed low for the known sources of error (source confusion, background estimation biases, data corruption, and calibration and zero point magnitude errors, as described in Cutri et al. (2012)), so we introduced an artificial error floor of 10%.

2.2. *MaNGA*

MaNGA (Mapping Nearby Galaxies at Apache Point Observatory) collects spatially-resolved spectra for 11,465 galaxies (Bundy et al. 2015). This is accomplished using fiber-bundle integral field units. The most meaningful emission lines for analyzing star formation are $H\alpha$ and $H\beta$, both of which are obtained for all galaxies in the MaNGA survey. Additionally, the MaNGA observations contain stellar velocity estimates in each spaxel, which are useful in determining if observed rejuvenation in the SFR could be caused by a merger or other disturbance. The other spectral lines observed

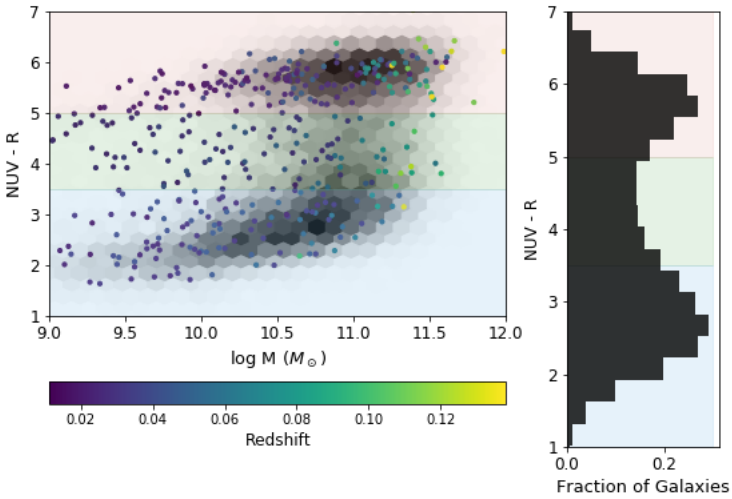

Figure 1: Color-mass diagram for GSWLC-Deep galaxies within $z = 0.14$. The underlying hex histogram contains all galaxies within this redshift in GSWLC-Deep, and the overlaid dots are the galaxies that are also in the MaNGA catalog, colored by redshift. ($z = 0.14$ was chosen because 0.14 is the maximum redshift in the MaNGA sample.) The bimodality in the right panel demonstrates the origin of the term 'green valley'.

from MaNGA could be useful in future related work to use BPT diagrams to determine if there is an active galactic nucleus in a specific galaxy.

2.3. *Sample Selection*

For this analysis, we choose to only use galaxies that have deep UV photometry by using the GSWLC-Deep catalog that contains 48,401 galaxies covering 7% of SDSS (Salim et al. 2018). In total, using catalog release 2.4.3 from MaNGA, there are 433 common galaxies with the GSWLC-Deep catalog, matched by constraining the sky coordinates to be within 0.5". The Deep catalog is chosen because it has the highest quality UV photometry, with UV exposure times of at least 4000s. These reliable UV measurements are important to infer accurate SFRs and dust attenuation, which is key for accurately fitting the SED as a whole.

Figure 1 shows the distribution of galaxies by mass and NUV-R color. The underlying grayscale shows the distribution of the all galaxies included in the GSWLC-Deep catalog, and the overlaid dots are the individual galaxies that are in both MaNGA and GSWLC-Deep. By selecting only galaxies that are in MaNGA, we inherently choose a redshift cutoff of $z < 0.15$. One feature of note in Figure 1 is that the selection of only low-redshift galaxies likely also favors lower-mass galaxies, as can be seen by the concentration of the points toward masses on the order of $10^{10} M_\odot$. MaNGA additionally tries to evenly sample galaxies across different colors, so it also favors green valley galaxies.

3. PHYSICAL MODEL DESCRIBING A GALAXY

To model the spectral energy distribution of a galaxy, we need to quantify the parameters that influence the shape and features of the SED. Our model is very similar to that described in Leja et al. (2017). The parameters that go into the model are described below.

3.1. *Stellar population model*

The stellar population model in this SED modeling procedure is flexible for a variety of initial mass functions and metallicities. The underlying framework for the stellar population modeling used in this work is Flexible Stellar Population Synthesis (implemented in python with python-FSPS) (Conroy & Gunn 2010,?; Foreman-Mackey et al. 2014). This allows us to compute simple stellar populations (SSPs). The metallicity of the stellar population is important because it informs the ratio between the fluxes at optical and Near-IR wavelengths. Prospector models metallicity with a distribution rather than discretely, and there is no implemented age-metallicity relationship. The FSPS model has been shown to compare favorably to other stellar population synthesis models, especially when fitting ultraviolet data (Conroy & Gunn 2010).

3.2. *Star-formation History*

Our model fits the star-formation histories non-parametrically, using 8 time bins to determine the star formation rate during each time bin that yields the most likely set of parameter values for the observed SED. A non-parametric fit to the star formation history is preferable because it doesn't include many of the systematic uncertainties and errors that are involved in a parametric fit (Conroy 2013). For the relatively small sample of galaxies in this work, the computational cost of fitting non-parametric star formation histories is not a limiting factor.

The times in the star formation history are lookback times. The non-parametric star formation history is created by comparing the star formation rate in each time bin to the star formation rate in the adjacent time bins. At more distant times, the resolution becomes poorer and the time bins become larger. N (in this case, 8) time bins are used in the nonparametric SFH model. Two bins are fixed at 0-30 Myr and 30-100 Myr to capture variations in the recent SFH of galaxies. A third bin is placed at $0.85t_{univ} - t_{univ}$, where t_{univ} is the age of the universe at the observed redshift, to model the oldest possible population. The remaining five bins are spaced equally in logarithmic time between 100 Myr and $0.85t_{univ}$.

3.3. *Dust Attenuation and Emission*

In this model, the dust attenuation curve is flexible and attenuates all other emission modeled from the galaxy. The dust attenuation, τ_ν, caused by the dust in the birth-cloud and the dust attenuation caused by the presence of diffuse dust are often degenerate (Leja et al. 2017). The ratio between the attenuation caused by the birth-cloud and the attenuation the diffuse dust is also fit. There is additionally a parameter (dust index) that describes the slope of our assumed Kriek & Conroy (2013) dust attenuation curve and is also related to the strength of the UV bump.

Dust emission is modeled assuming energy balance, meaning that the dust emits in the infrared all the energy it receives from the stars in the galaxy at all wavelengths (da Cunha et al. 2008). This substantially contributes to the amount of infrared emission modeled in the SED. Three parameters constrain the dust emission in our model: U_{min}, γ, and Q_{PAH}. U_{min} is the minimum starlight intensity the dust receives, γ is the fraction of the dust that receives this light, and Q_{PAH} represents the amount of the dust that consists of a certain compound that is known to have strong features in the mid-infrared (Leja et al. 2017).

3.4. *AGN Model*

The presence of an active galactic nucleus obscured by dust would significantly influence the mid-infrared flux produced by the warm dust surrounding the AGN. The impact of an active galactic nucleus is factored into this model. The inclusion of AGNs in modeling the SED significantly improves the predictions of important emission lines like $H\alpha$ and $H\beta$, as well as changing the derived stellar ages, SFRs, and dust attenuations (Leja et al. 2018).

4. SED FITTING

The spectral energy distribution of a galaxy contains the most complete set of information about that galaxy, including the current stellar population, the star-formation history, dust, and gas. Fitting a spectral energy distribution can therefore give the most information about the properties of a galaxy. This Bayesian fitting algorithm attempts to resolve some of the degeneracies between parameters, when used with the dynesty nested sampling algorithm to explore the parameter space (Speagle 2019). To create the desired non-parametric star formation histories, it is crucial to use a Bayesian method of analysis (like that in Prospector) because of the high level of degeneracy between some parameters. In general, our SED fitting procedure follows that described in Leja et al. (2017). The specifics of this are described below.

4.1. *Prospector Run*

We ran Prospector (Johnson & Leja 2017) on the spectral energy distributions of the 433 galaxies that were found to be in both GSWLC and the MaNGA catalog. Table **??** contains the most pertinent information about the key parameters.

Our model includes 3 free parameters for dust attenuation, 3 free parameters for dust emission, multiple free parameters for the stellar population, 7 parameters for the star formation history, and 2 parameters for the AGN. The dust modeling parameters are τ_ν, dust ratio, and the dust index. τ_ν represents the dust attenuation caused by diffuse dust. The dust ratio represents the ratio between the birth cloud dust attenuation and the diffuse dust attentuation. The dust index represents the power-law multiplier to the Calzetti et al. (2000) attenuation curve. The stellar population free parameters most notably include the metallicity, expressed as $log(\frac{Z}{Z_\odot})$, and the total mass formed, expressed as $log(\frac{M}{M_\odot})$. To create the star formation history, there are 7 different SFR ratios where the SFR in a time bin is compared to the SFR in the adjacent time bins (in this case, we used 8 bins.) The AGN is modeled by two parameters: fAGN, which represents the fraction of the bolometric flux that is caused by the AGN, and τ_{AGN}, which represents the optical depth of the dust in the torus surrounding the AGN. The three parameters for dust emission are U_{min}, γ, and Q_{PAH}. U_{min} is the minimum starlight intensity the dust receives, γ is the fraction of the dust that receives this light, and Q_{PAH} represents the amount of the dust that consists of polycyclic aromatic hydrocarbons, which are known to contribute significantly to the mid-infrared (Leja et al. 2017).

4.2. *Priors*

Weakly informative priors were selected for each parameter. Information on key parameters and their priors is summarized in Table 1.

The prior for the mass formed is uniform from $9 < log(\frac{M}{M_\odot}) < 12.5$. The prior for metallicity is uniform from $-1 < log(\frac{Z}{Z_\odot}) < 0.3$. The prior for the dust attenuation from diffuse dust (τ_ν) is a clipped normal distribution with a maximum of 4.0, a minimum of 0.0, a mean of 0.3, and a standard deviation of 1.0. The dust ratio prior is a clipped normal distribution with a maximum of 2.0, a

Table 1: Key Parameters and Priors

Parameter	Description	Prior
Mass: $\log(\frac{M}{M_\odot})$	Total stellar mass formed	Uniform between 9 and 12.5
Metallicity: $\log(\frac{Z}{Z_\odot})$	Metallicity of stellar population	Uniform between -1 and 0.3
SFR Ratios	Ratio of the SFRs in adjacent bins of the 8-bin nonparametric SFH	Students-t distribution (Leja et al. 2019)
f_{AGN}	Fraction of the total bolometric luminosity contributed by AGN	Log-uniform between 10^{-5} and 3
τ_{AGN}	Optical depth of the dust torus surrounding AGN	Log uniform between 5 and 150
τ_ν	Dust attenuation caused by diffuse dust	Clipped normal with $\mu = 0.3$ and $\sigma = 1.0$
Dust Ratio	Ratio between attenuation by birth cloud and attenuation by diffuse dust	Clipped normal with $\mu = 1.0$ and $\sigma = 0.3$
Dust index	Power law multiplier to dust attenuation curve	Uniform between -2 and 0.5
U_{min}	Minimum starlight intensity	Clipped normal with $\mu = 1.0$ and $\sigma = 0.5$
γ	Fraction of dust receiving starlight	Log uniform between 10^{-3} and 10^{-1}
Q_{PAH}	Amount of PAH	Uniform between 0.5 and 7

minimum of 0.0, a mean of 1.0, and a standard deviation of 0.3. The dust attenuation index, n, has a flat uniform prior between $-2 < n < 0.5$. The prior for U_{min} is a clipped normal distribution ith a maximum of 25.0, a minimum of 0.1, a mean of 1.0, and a standard deviation of 0.5. For γ, the prior is log uniform between 10^{-3} and 10^{-1}. The prior for Q_{PAH} is flat uniform between $0.5 < Q_{PAH} < 7$. The fAGN prior is log uniform between $10^{-5} < f_{AGN} < 3.0$. The prior for τ_{AGN} is log uniform between $5 < \tau_{AGN} < 150$. The prior for the ratio between the star-formation rates in adjacent time-bins is the continuity prior described in §2.2.3 of Leja et al. (2019). This prior fits directly for the change in $log(SFR)$ between adjacent time bins, and attempts to minimize sharp jumps in the SFR as a function of time.

5. RESULTS

From the 433 galaxies that are in both the MaNGA and GSWLC samples, 249 of them were considered satisfactory fits, based on both the fit converging and a χ^2 value between 0.3 and 3. Because we will classify galaxies by their NUV-R color, we eliminate galaxies that don't have near-UV photometry, and 225 remain. To select the galaxies that are considered to lie in the 'green valley', we used a cutoff in NUV - R color of 3.5 to 5. Using this cutoff, our sample contains 61 green valley galaxies, The reasoning behind this cutoff can be seen in the histogram in Figure 1; the green shaded region represents this intermediate region between the blue galaxies and the red galaxies. Choosing galaxies as green valley based on color is the most conventional metric, and we will discuss later some of the potential issues with this choice. To attempt to distinguish between a galaxy's color and its star formation, we classify galaxies separately by color and by sSFR. We consider all galaxies in our sample with a NUV-R color less than 3.5 ($n = 70$) to be blue, which would conventionally be assumed to be star-forming, and all galaxies with a NUV-R color greater than 5 ($n = 94$) to be red,

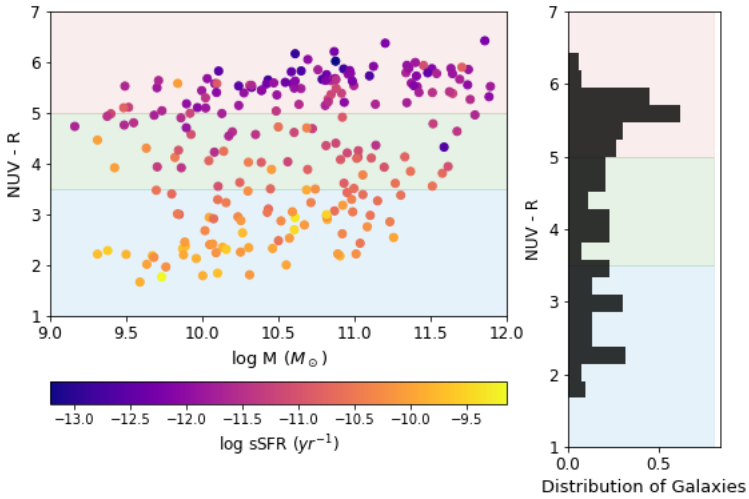

Figure 2: Color-mass diagram for the successfully fitted galaxies. The same bimodality seen in Figure 1 is not seen here, due to the smaller number of galaxies and the selection effects of the MaNGA catalog's preferential selection of low-mass and green valley galaxies.

and conventionally assumed to be quiescent.

As a result of the SED fitting, however, we are able to make a more accurate classification of the star formation taking place in a galaxy than can be made by color alone. Our classification of galaxies as star-forming, transitional, or intermediate is based on the sSFR within the last 1 Gyr. Galaxies with a sSFR greater than $10^{-10.6}yr^{-1}$ ($n = 77$) are considered star-forming. Galaxies with a sSFR less than $10^{-10.6}yr^{-1}$ ($n = 98$) are considered quiescent. Galaxies with sSFRs between those values ($10^{-10.6}yr^{-1} > sSFR_{trans} > 10^{-10.6}yr^{-1}$) ($n = 50$) are considered to be transitional. These cutoffs are chosen such that galaxies we define as star-forming at least double their mass within 3 times the Hubble time, and quiescent galaxies do not double their mass within 20 times the Hubble time. Transitional galaxies are those with mass-doubling timescales between 3 and 20 times the Hubble time.

Combining these two classification systems allows us to determine how many of the green galaxies in our sample are star-forming, transitional, or quiescent. We find that 49% of the green valley galaxies in our sample are transitional ($n = 30$), 23% are star-forming ($n = 14$), and 28% are quiescent ($n = 17$).

Figure 2 shows that the specific star formation rates generally follow the expected gradient, where galaxies with a bluer NUV-R color show higher rates of star formation than the galaxies with a redder color.

Figure 3 shows the distribution of the galaxies in our sample. This plane mostly shows the expected pattern of blue galaxies having higher sSFRs than their green valley or red counterparts. However, most notably, there are exceptions to this, which indicates the inherent inaccuracies in classifying a galaxy's star formation from its color. These include both dust attenuation and metallicity and are discussed in more depth in Section6. This demonstrates why we classify galaxies as star-forming, transitional, or quiescent based on their sSFR instead of their color.

Figure 4 shows the roughly linear relationship between the present sSFR of a galaxy and its color. It

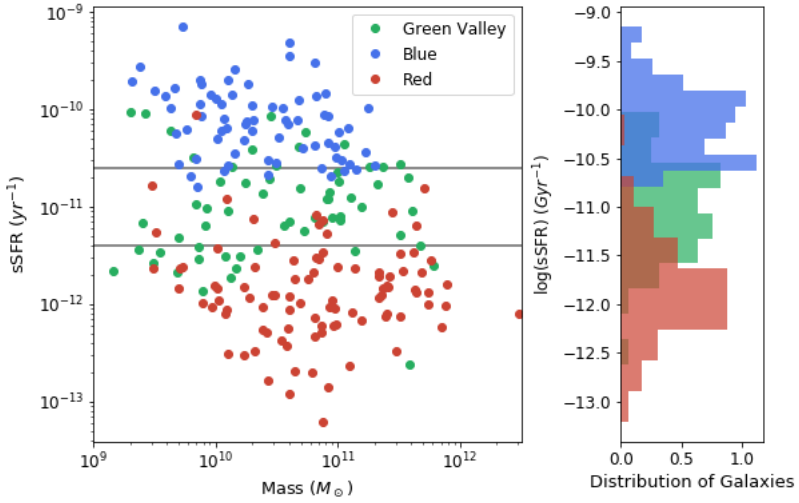

Figure 3: The distribution of galaxies in the sSFR-mass plane, colored by their NUV-R color. Note that the galaxies selected as green valley by color also are concentrated in intermediate values of sSFR. The horizontal lines represent the cutoff values of sSFR used to classify galaxies as star-forming, transitional, or quiescent.

is known that the presence of dust causes an object to appear artificially red. This poses a problem when attempting to use color to determine whether or not a galaxy is star-forming, because a star-forming galaxy with a high amount of dust may have the same NUV-R color as an intermediate green valley galaxy with little dust. The gradient seen in the dust attenuations in Figure 4 indicates that for a given NUV-R color, dust is a significant contributing factor to the spread of specific star formation rates.

Figure 5 shows the gradient in the ratio of the sSFR 100 Myr ago compared to the sSFR 1 Gyr ago. Values greater than one indicate that the star formation is increasing with time toward the present epoch, and values less than one indicate that the star formation is decreasing. The distribution of ratio values is shown in Figure 6. It is clear that generally, blue galaxies appear to be slowing their star formation less quickly than green or red galaxies. It is of note that the green valley galaxies seem to be concentrated in the central values of the sSFR. The mean green valley sSFR is $1.5 \times 10^{-11} yr^{-1}$, which corresponds to a mass doubling timescale of approximately 64 Gyr (which is significantly longer than the Hubble time). For the 61 green galaxies in our sample, the median ratio of $\frac{sSFR_{100Myr}}{sSFR_{1Gyr}}$ is 0.59 ± 0.20. The median $\frac{sSFR_{100Myr}}{sSFR_{1Gyr}}$ ratio for blue galaxies in our sample was 0.85 ± 0.19, and for red galaxies was 0.48 ± 0.20. We expect that all galaxies, regardless of color, will show a general trend of decreasing star formation, because we know that star formation has been decreasing since $z = 2$ (Ilbert et al. 2015). Our results are consistent with this expectation, because the median ratios for all galaxy colors are less than one. Comparing the sSFR ratios also allows us to state that from the median values, green galaxies are decreasing their star formation about 30% faster than their blue counterparts. (Comparing the ratios based on the sSFR classifications of quiescent, transitional, or star-forming yields no significantly different results; any galaxies that experience unexpected star formation for their color don't significantly affect the medians computed for each color sample.)

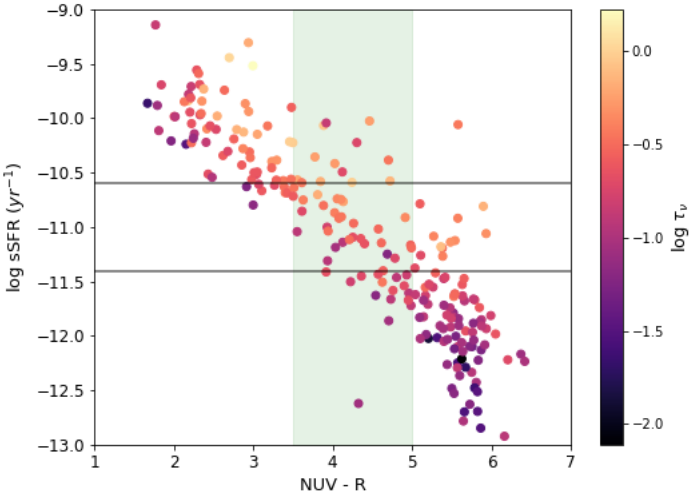

Figure 4: The distribution of the full fitted sample of galaxies by sSFR and NUV-R color. The color of the dots represents the dust attenuation, τ_ν, where higher values represent more dust and therefore a higher degree of reddening. The horizontal lines represent the sSFR cutoffs for star-forming (above the upper horizontal line) and quiescent galaxies (below the lower horizontal line).

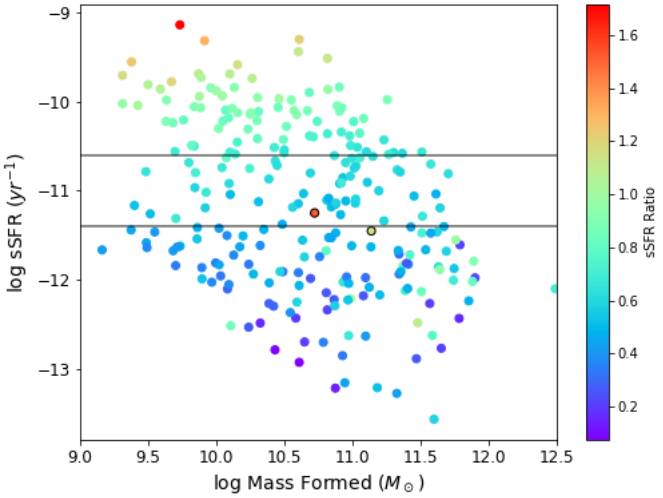

Figure 5: The distribution of galaxies in the sSFR-mass plane, where the color indicates the ratio between the sSFR 100Myr ago and the sSFR 1Gyr ago, which indicates whether star formation is increasing or decreasing in the galaxy. The horizontal lines represent the sSFR cutoffs for star-forming (above the upper horizontal line) and quiescent galaxies (below the lower horizontal line). The circled points represent galaxies with unusually high ratios for their location on the sSFR-mass plane; these are discussed in more depth in Section 5.1

.

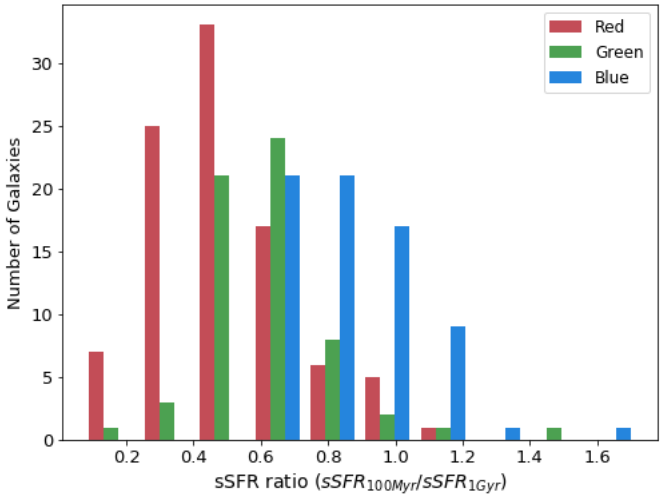

Figure 6: Distribution of sSFR ratios between 100Myr ago and 1 Gyr ago, by NUV-R color. Bluer galaxies are shown to have higher sSFR ratios, meaning that their star formation is not decreasing as quickly as their green or red counterparts.

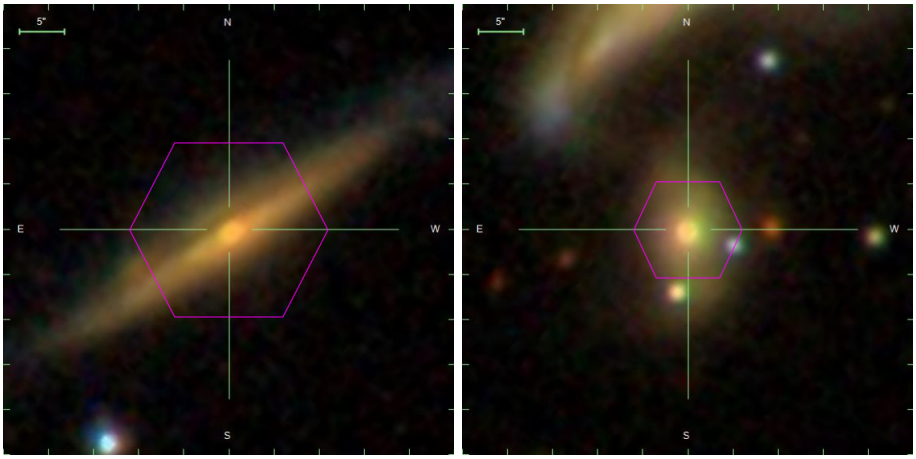

Figure 7: Optical images of the two possibly-rejuvenating galaxies observed in this sample.

The circled points in Figure 5 are the two galaxies in this sample that appear to have an increasing sSFR, as shown by their ratio being greater than one. These would be the galaxies we consider to be candidates for "rejuvenation", and are described more in Section 5.1.

5.1. *Example: Possibly Rejuvenating Galaxies*

The two green valley galaxies circled in Figure 5 have unusually high sSFR ratios compared to other galaxies in approximately the same location on the sSFR-mass plane. This motivated us to analyze other properties of these galaxies. This section outlines some examples of how MaNGA data provides a useful follow-up to noTable properties observed from SED fitting. Figure 7 shows the optical images, obtained from MaNGA, of the two galaxies observed to have these unusually high sSFR ratios. Figure 8 shows the star formation history and the estimated mass and sSFR of these

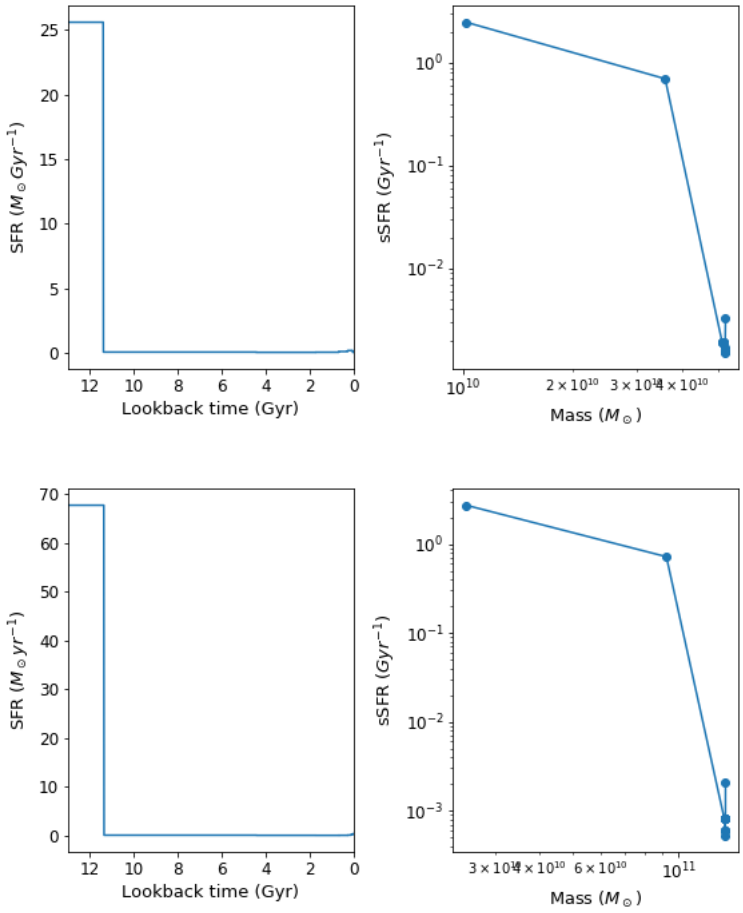

Figure 8: *Left Panel:* Non-parametric star formation history: The star formation rate as a function of time, fitted with 8 bins. *Right Panel:* The progression over 13 Gyr of this individual galaxy in the sSFR-Mass plane.

galaxies over 13 Gyr.

As shown in Figure 8, both green valley galaxies with high sSFR ratios have star formation histories from our model that are essentially flat for the majority of the age of the universe and then experience an uptick in star formation in the last billion years or so. Further analysis, including varying the number of star-formation history bins, would be required to know if the SFH seen here is realistic. We expect rejuvenating galaxies to show a region of bright central $H\alpha$ emission from cosmological models (Tacchella et al. 2016). Figure 9 shows the $H\alpha$ and $H\beta$ emission maps for one of the rejuvenating galaxies in our sample; it appears that the $H\alpha$ emission is indeed centrally concentrated.

5.2. *Example: A Dusty Star-Forming Galaxy*

As discussed previously, the green valley defined by color contains a significant number of dusty star forming galaxies. In this section, we focus on one example of this and show how the results from Prospector help us to have a stronger understanding of the properties of this galaxy than we would have from its photometry alone.

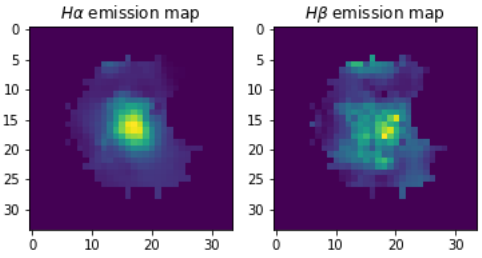

Figure 9: $H\alpha$ and $H\beta$ emission maps, from MaNGA, for one of the rejuvenating galaxies discussed in this section. Note the centrally concentrated $H\alpha$ emission.

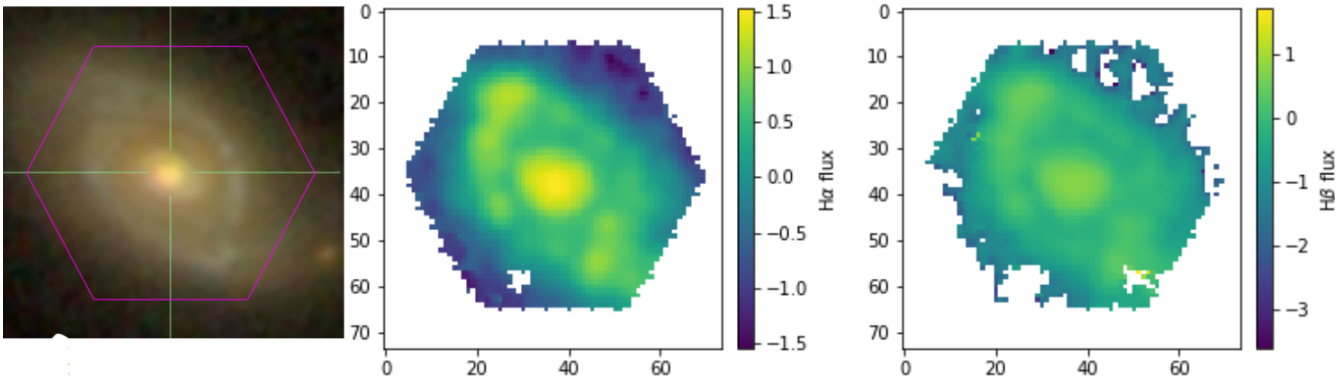

Figure 10: Optical, $H\alpha$, and $H\beta$ maps of the dusty star-forming galaxy described in Section 5.2

Figure 10 shows the optical image, as well as the $H\alpha$ and $H\beta$ emission line maps obtained from MaNGA of this galaxy. The bright $H\alpha$ emission seen in the spiral arms indicates the presence of star formation. This galaxy has a dust attenuation of 0.57, an NUV-R color of 3.779 (placing it squarely in the green valley, based on our color classification scheme). The sSFR is $10^{-10.3}yr^{-1}$, and its current mass is approximately $10^{11}M_{\odot}$. Figure 11 shows the progression of this galaxy in the sSFR-Mass plane over the last 13 Gyr of time. Figures like figures 8 and 11 enable us to understand the timescales of star formation, quenching, and rejuvenation estimated by our model.

6. DISCUSSION AND FUTURE WORK

The spectral energy distribution contains the most comprehensive information about all the different component parts of a galaxy. Fitting with Prospector allows us to fit separately for the effects of parameters that are known to be degenerate, like metallicity, dust, and the age of the stellar population. The SED fits performed with Prospector show that dust attenuation is a more substantial contributor to reddening of star-forming or green-valley galaxies than differences in stellar metallicity. However, there is still a slight degeneracy between dust and metallicity even with Prospector, so further analysis is necessary.

Selecting our population of green valley galaxies by color is the most appropriate when one considers the conventional use of the term green valley and its origin from the color-magnitude diagram. However, this work shows that due to dust attenuation, it is not necessarily appropriate to assume

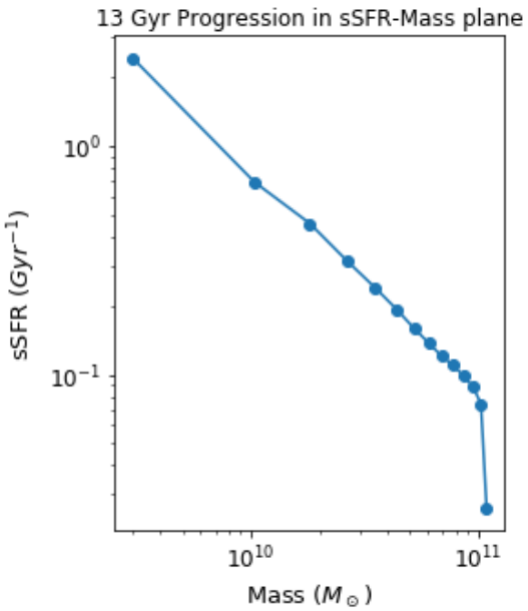

Figure 11: The progression of the dusty star forming galaxy over 13 Gyr of cosmic time. It begins in the upper left corner with a lower mass but a higher sSFR, and progresses toward the lower right over time, with the lowest dot representing the galaxy as we observe it today.

that the color of a galaxy is a true indicator of the properties of its stellar population, or of the presence or absence of star formation. It is likely that some galaxies selected as green valley in this work are actually star-forming galaxies that have high levels of dust attenuation. It is also likely that there are galaxies that are in an intermediate stage between star-forming and quiescent, but have an artificially red color due to dust attenuation, and therefore are not labeled as green valley when the selection is made by color.

Additionally, the selection of only galaxies with UV photometry has likely biased our sample in some way. However, at this stage, it is not clear what that bias is or how it influences our results. In future work, we hope to perform further analysis that allows us to determine the influence of the UV selection bias.

Selecting only galaxies that are in the SDSS MaNGA survey biases our sample toward low mass, low redshift galaxies, and includes an unusually high number of green valley galaxies. In future work, the results of MaNGA-included galaxies could be compared against the results from the whole GSWLC catalog to see if the selection effects of using MaNGA galaxies bias our results.

It is also known that the presence of active galactic nuclei can influence the flux produced by galaxies at a wide range of wavelengths. Our model includes the influence of an AGN at long wavelengths by estimating the percentage of the flux that's caused by an AGN, but this is only a very rough approximation for the influence of an AGN on the spectral energy distribution. However, in this sample, our model claims that only 7 galaxies had greater than 5% of their flux produced by an AGN, and for that reason we do not attempt to make claims about galaxies with active galactic nuclei. Future analysis could use the additional information provided by MaNGA to create a BPT diagram for our sample of galaxies and determine the presence of an AGN from that, instead of solely relying on the model's estimate of the role an AGN would play (quantified by the fAGN parameter). Additionally, if the methods of this work were repeated on a larger sample, it is likely there would

be more galaxies with a higher fAGN value, which would possibly allow for conclusions to be drawn about the role of AGN in star formation histories.

The same methods used in this work could be applied to a larger catalog of galaxies from GSWLC-Medium or GSWLC-All-sky. More general statements would be able to be made from a larger sample of galaxies. There are 2259 common galaxies between MaNGA and the GSWLC-Medium catalog, compared to the 433 overlapping galaxies between MaNGA and GSWLC-Deep used in this analysis. However, the lower quality UV photometry in the Medium or All-sky catalogs may lead to significantly increased uncertainties, especially in relation to the star formation rates and the amount of dust attenuation. Because these are key parameters to draw conclusions from, it is unclear how advantageous the use of these larger but less precise catalogs would be.

In future analysis, we hope to vary the number of star formation history bins used in the SED fitting to attempt to account for features in the SFH that may be artificial and only caused by the time-binning used in this fit.

Spatially resolving star formation using MaNGA spectra and comparing to the SFR information output by Prospector is one of the most exciting future applications of this work. With this, we can investigate both centrally concentrated rejuvenation and inside out quenching (Tacchella et al. 2016; Pan et al. 2014). Further related analysis of the star formation histories could also attempt to quantify how long we expect galaxies to spend in the green valley before their star formation stops entirely and they become quiescent red galaxies. Other research suggests that massive red sequence galaxies form first (Gonçalves et al. 2012), and we could test this by comparing the timescales of quenching for galaxies of different masses.

7. CONCLUSIONS

Using the Bayesian inference machine Prospector, we fit the spectral energy distributions of 249 galaxies from the GSWLC-Deep catalog, selected based on their inclusion in the SDSS MaNGA sample. We analyze the impact of dust attenuation on classifying galaxies' star formation by their color, and discuss a variety of future work and applications that can follow from the results of using Prospector on the GSWLC in combination with MaNGA's spatially resolved spectra.

Overall, it appears that the green valley galaxies in this sample are generally quenching, or reducing their star formation, but at only 30% more quickly than their bluer counterparts. This supports the conventional idea that galaxies progress from blue, star-forming galaxies to red, quiescent galaxies by passing through the green valley. However, even in our small sample, there are still galaxies that appear to have unexpected amounts of star formation compared to other galaxies that share many of their properties. Future work could include selecting these individual candidate galaxies and analyzing their spatially-resolved spectra from MaNGA to determine possible explanations for their unusual properties.

By comparing the classification of galaxies by color and by sSFR, we show that although color does generally agree with the sSFR classification, it is subject to the influence of dust attenuation and stellar metallicity, and for this reason, classifying galaxies by their sSFR is more useful. The conventional category of "green valley" is likely contaminated with many dusty star-forming galaxies, but using Bayesian SED fitting allows us to estimate a galaxy's star formation independent of its color.

REFERENCES

Baldry, I. K., Glazebrook, K., Brinkmann, J., et al. 2004, ApJ, 600, 681

Bundy, K., Bershady, M. A., Law, D. R., et al. 2015, ApJ, 798, 7

Calzetti, D., Armus, L., Bohlin, R. C., et al. 2000, ApJ, 533, 682

Conroy, C., & Gunn, J. E. 2010, ApJ, 712, 833

Conroy, C., & Gunn, J. E. 2010, FSPS: Flexible Stellar Population Synthesis, ascl:1010.043

Conroy, C. 2013, ARA&A, 51, 393

da Cunha, E., Charlot, S., & Elbaz, D. 2008, MNRAS, 388, 1595

Cutri, R. M., Wright, E. L., Conrow, T., et al. 2012, Explanatory Supplement to the WISE All-Sky Data Release Product

Foreman-Mackey, D., Sick, J., & Johnson, B. 2014, Python-Fsps: Python Bindings To Fsps (V0.1.1), v0.1.1, Zenodo, doi:10.5281/zenodo.12157

Gonçalves, T. S., Martin, D. C., Menéndez-Delmestre, K., et al. 2012, ApJ, 759, 67

Ilbert, O., Arnouts, S., Le Floc'h, E., et al. 2015, A&A, 579, A2

Johnson, B., & Leja, J. 2017, Bd-J/Prospector: Initial Release, v0.1, Zenodo, doi:10.5281/zenodo.1116491

Kriek, M., & Conroy, C. 2013, ApJL, 775, L16

Leja, J., Johnson, B. D., Conroy, C., et al. 2017, ApJ, 837, 170

Leja, J., Johnson, B. D., Conroy, C., et al. 2018, ApJ, 854, 62

Leja, J., Johnson, B. D., Conroy, C., et al. 2019, ApJ, 877, 140

Leja, J., Carnall, A. C., Johnson, B. D., et al. 2019, ApJ, 876, 3

Pan, Z., Li, J., Lin, W., et al. 2014, ApJL, 792, L4

Salim, S., Lee, J. C., Janowiecki, S., et al. 2016, ApJS, 227, 2

Salim, S., Boquien, M., & Lee, J. C. 2018, ApJ, 859, 11

Speagle, J. S. 2019, arXiv e-prints, arXiv:1904.02180

Strateva, I., Ivezić, Ž., Knapp, G. R., et al. 2001, AJ, 122, 1861

Tacchella, S., Dekel, A., Carollo, C. M., et al. 2016, MNRAS, 458, 242